ADVANCED FUNCTIONAL MATERIALS
www.afm-journal.de

Sustainable Spinning of Artificial Spider Silk Fibers with Excellent Toughness and Inherent Potential for Functionalization

*Ruxia Fan, Katarina Knuuttila, Benjamin Schmuck, Gabriele Greco, Anna Rising, Markus B. Linder, and A. Sesilja Aranko**

Despite impressive progress in the field, there are still several major bottlenecks in producing fibers from recombinantly produced spider-silk-like proteins to replicate the extraordinary mechanical properties of spider major ampullate silk. The conventional artificial fiber spinning processes rely primarily on organic solvents to coagulate proteins into fibers and require complex post-treatments to obtain fibers with valuable properties. This is due to challenges in obtaining soluble silk proteins, but also because the native silk spinning process leading to the hierarchical organization of the silk proteins is not fully understood and is hard to replicate in a manner applicable to industrial settings. Here, recombinant spider-silk fusion proteins are efficiently produced and processed into as-spun fibers with a toughness modulus of 120 MJ m^{-3} and extensibility of 255% using solely aqueous solutions. The spider-silk fusion proteins assemble in a manner similar to that reported for native spider silk: they phase separate induced by salting out, followed by alignment and a secondary structure transition triggered by shear forces and dehydration. Finally, the design of the fusion silk proteins enables straightforward functionalization of the fibers under mild all-aqueous conditions via a simple biomolecular click reaction both pre- and post-spinning.

1. Introduction

Spider silks harbor unusual mechanical properties, combining remarkable strength and extensibility.[1] These features, along with biodegradability, make spider silk appealing for many applications, such as textiles, automotive, defense, and healthcare.[2–5] Thus, spider silk has the potential to serve as a sustainable alternative to many petroleum-based fibers which are increasingly becoming environmental problems due to their non-renewable nature and poor biodegradability.[4,6,7]

The high performance of spider silks derives from their complex hierarchical substructure.[8] The two key factors behind this are the unique molecular structure of native spider silk proteins, called spidroins, and the highly sophisticated spinning process of spiders that takes place under mild conditions, driven by chemical triggers and physical force.[9–11] Some spidroins from major ampullate glands (MaSps) have molecular masses of over 250 kDa and share a common architecture, an extensive repetitive region flanked by a non-repetitive amino-terminal domain (NTD) and a carboxyl-terminal domain (CTD).[10,12] The mechanical properties of spider silks are mainly determined by the intermediate repeat region which contains two alternating motifs. According to the current model, poly-alanine regions form β-sheet crystalline structures that are essential for the strength of the fibers, while glycine-rich regions form amorphous chains providing the extensibility.[13–16] The non-repetitive terminal domains maintain the solubility of spidroins in the gland and then ensure proper alignment and polymerization of spidroin molecules by responding to various physicochemical factors during the complex spinning process.[10,17–26]

Recombinant production of spider silk-like proteins is considered an effective approach to produce high-strength man-made fibers. However, the high-molecular weight spider-silk proteins have poor yield and solubility. Thus, the purification and fiber-spinning processes of recombinant silk proteins typically require denaturing agents such as urea and guanidinium, or organic solvents like hexafluoro isopropanol, methanol, ethanol,

R. Fan, K. Knuuttila, M. B. Linder, A. S. Aranko
Department of Bioproducts and Biosystems
School of Chemical Engineering
Aalto University
P.O. Box 16100, Espoo FI-02150, Finland
E-mail: sesilja.aranko@aalto.fi

B. Schmuck, G. Greco, A. Rising
Department of Animal Biosciences
Swedish University of Agricultural Sciences
Box 7011, Uppsala 75007, Sweden

B. Schmuck, A. Rising
Department of Medicine Huddinge
Karolinska Institutet
Neo, Huddinge 14186, Sweden

The ORCID identification number(s) for the author(s) of this article can be found under https://doi.org/10.1002/adfm.202410415

DOI: 10.1002/adfm.202410415

and isopropanol.[27–35] Low production yield and the use of harsh solvents hinder the industrial applications and sustainability of the process. As an attractive alternative, an entirely aqueous spinning strategy based on a recombinant mini-spidroin fused with NTD and CTD can be employed and has been reported to result in artificial fibers with attractive mechanical properties.[36–38] The terminal domains, especially the NTDs, are essential for the generation of fibers in this aqueous biomimetic spinning system.

Here, we report that recombinant spider silk-like proteins flanked by globular terminal domains that enable functionalization instead of the NTD and CTD. These fusion proteins can be produced in a soluble manner in high yields and be spun into tough and extensible fibers via an aqueous spinning method. The assembly of the spider silk-like fusion proteins is based on salting out and thus differs from the previously reported aqueous spinning method of silk-mimicking proteins that is triggered by a change in pH leading to polymerization and conformational changes of NTD and CTD. Our data shows that the assembly process of the spider silk fusion protein ultrastructurally resembles that of native spider silk and highlights the role of phase separation in the spinning process. Furthermore, we show that the intrinsic capabilities of the terminal domains provide an opportunity for specific and simple single-step functionalization of the fiber under mild conditions via a biomolecular click reaction.

2. Results and Discussion

2.1. Recombinant Spider Silk Protein Design and Construction

We constructed a spider-silk fusion protein by fusing a 43 kDa fragment of a wild-type spidroin repetitive sequence from *Araneus diadematus*, ADF3, [39] with two SpyCatcher2 [40] domains to create SpyC-ADF3-SpyC (**Figure 1A**). Fusing a truncated spidroin repetitive sequence with SpyCatcher2 domains has been shown to result in soluble expression,[39] and, indeed, soluble expression in high yield was obtained also here (Figure S1, Supporting Information). In addition, Catcher proteins can form an isopeptide bond with Tag peptides via an autocatalytic biomolecular click reaction [41] thus enabling specific covalent conjugation of proteins or peptides with the fusion protein (Figure 1B). As our aim was not to mimic the pH induced spinning of spiders, we did not include NTD and CTD in the fusion protein. We did, however, construct a control by fusing ADF3 with the native terminal domains of spider silk proteins, an NTD from *Euprosthenops australis* MaSp1,[42] and a CTD from *Araneus ventricosus* MiSp,[43] to construct NTD-ADF3-CTD. NTD-ADF3-CTD was poorly soluble when expressed in *Escherichia coli* at 30 °C (Figure S1B, Supporting Information). Decreasing the expression temperature improved the solubility, but the obtained yield remained modest, as ≈20 mg L^{-1} was obtained at 16 °C (Figure S1B, Supporting Information). The observed low yield and solubility could be due to an unfavorable combination of the repetitive sequence and the terminal domains used here, because especially the NTD is a known tag for enhancing the yield and solubility of poorly expressed proteins.[36,44,45] In order to study the role of the globular terminal domains in the salting-out-induced spinning process, we selected two more fusion proteins with different globular terminal domains. These were selected based on our previous studies, in which several non-native globular fusion proteins were reported to increase the yield and solubility of recombinant spider-silk fusion proteins.[2,39,46–48] We selected constructs with either another Catcher domain, SilkCatcher (SilkC),[47] or cellulose binding domain (CBM) [49] as terminal globular domains, to result in fusion protein constructs named SilkC-ADF3-SilkC and CBM-ADF3-CBM, respectively (Figure 1A). Both of these fusion proteins were expressed in *E. coli* in a soluble form with yields of 80–100 mg L^{-1} of purified protein from shake-flask culture (Figure S1, Supporting Information).

2.2. Salting-Out-Induced Phase Separation and Shear-Induced Crystallization

The effects of salting out and salting in on proteins, first observed by Hofmeister in 1888, are also significant in the context of the assembly of spider silk proteins.[48,50–54] In particular, kosmotropic salts have been reported to control the coacervation of recombinant spider silk proteins.[48] We selected the kosmotropic cation ammonium (NH_4^+) and kosmotropic anion phosphate (PO_4^{3-}), to investigate how the salting out affects the self-assembly of the four fusion proteins.

To visualize the effect of salts on the different proteins, optical microscopy was used to observe the self-assembly induced by the two salts at various salt concentrations, pH values, and protein concentrations (Figure 1C,D; Figures S2–S7, Supporting Information). Phase separation of SpyC-ADF3-SpyC took place in high salt and protein concentrations, while at low salt and protein concentrations, either clear solution or small amorphous aggregates were observed instead of phase separation (Figure 1C,D; Figure S2, Supporting Information). Liquid-liquid phase separation (LLPS) with slow coalescence formed using a high concentration (0.5 M) of potassium phosphate (Figure 1C-a), while decreasing the concentration of potassium phosphate triggered the formation of separated tiny droplets (Figure 1C-b,c). When the concentration of potassium phosphate was 0.02 M or lower, the solution remained clear (Figure 1C-d). In high concentration of ammonium acetate (2.5 M) and SpyC-ADF3-SpyC (10 mg mL^{-1}) dense droplets formed instead of LLPS (Figure 1D-e). The droplets aggregated rapidly into a percolated droplet network. The behavior is characteristic to viscoelastic phase separation (VPS) [55] to which we call these assemblies as a distinction to LLPS. Decreasing the protein concentration resulted in a sparse network of droplets (Figure 1D-f). In 1.25 M ammonium acetate, LLPS droplets with characteristic liquid-like properties including the potential to fuse formed (Figure 1D-g), while in low protein and salt concentration, clear solution or small aggregates were observed (Figure 1D-h). The VPS droplets were distinguished from LLPS droplets and aggregates by their inability to fuse and potential to form networks of droplets, respectively. Data from turbidity measurements is in line with the analysis by light microscopy (Figure S3, Supporting Information). Intermixing of the protein and salts resulted in an instant turbidity change. Ammonium acetate had a weaker effect than potassium phosphate at the same concentration but was more potent at higher concentrations.

SilkC-ADF3-SilkC, showed similar salting-out behavior to SpyC-ADF3-SpyC (Figure S4, Supporting Information), while the salting-out effect on CBM-ADF3-CBM was stronger than on SpyC-ADF3-SpyC and SilkC-ADF3-SilkC (Figures S5 and S6,

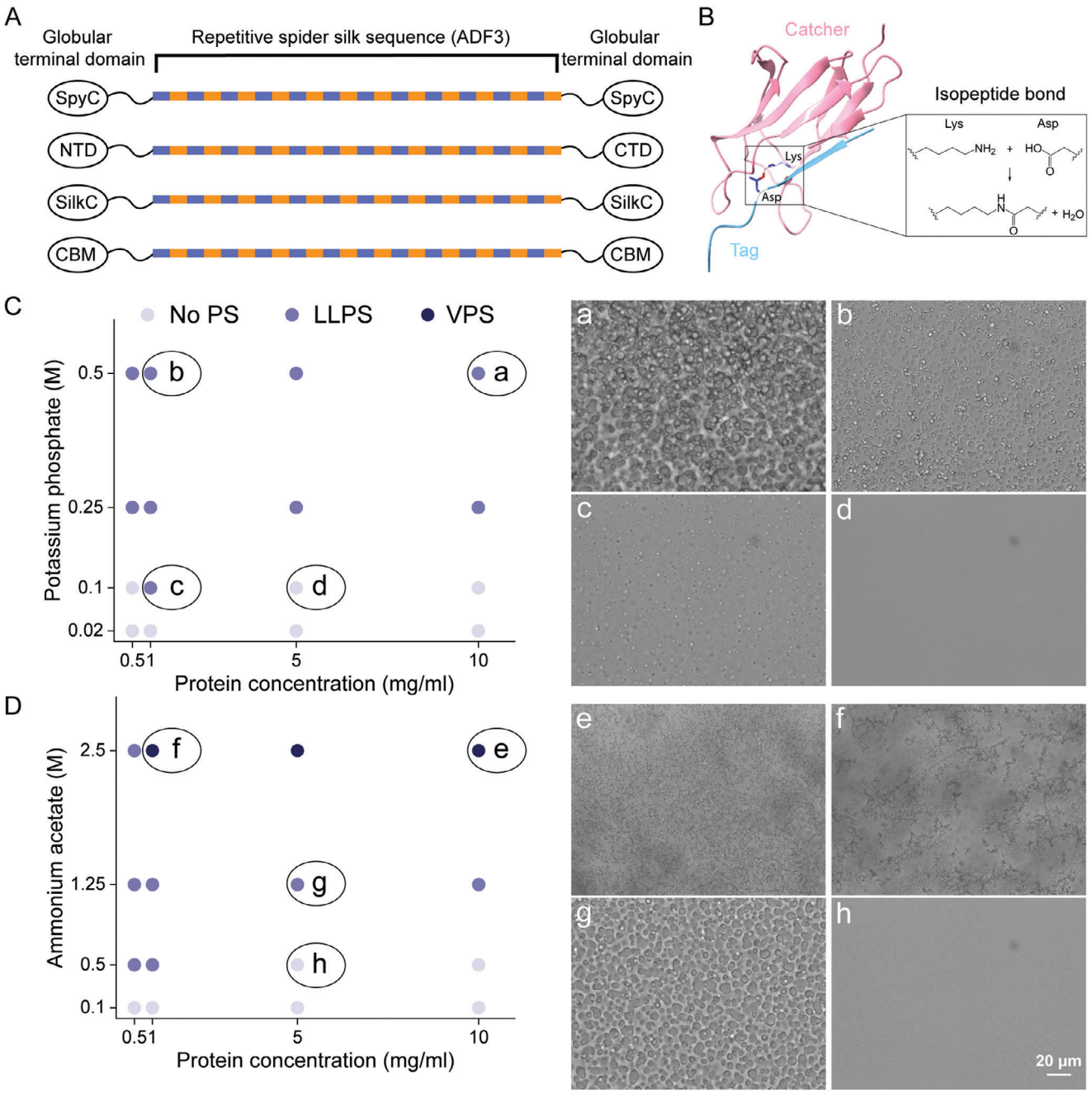

Figure 1. Construction of four fusion proteins and phase separation of SpyC-ADF3-SpyC. A) Schematic presentation of the designed recombinant spider-silk fusion proteins. B) Schematic of covalent isopeptide band formed between Catcher and Tag. C) Phase diagram and representative optical microscope images of SpyC-ADF3-SpyC protein under potassium phosphate buffer in pH 7.0. No PS stands for no phase separation, LLPS stands for liquid-liquid phase separation, VPS stands for viscoelastic phase separation. D) Phase diagram and representative optical microscope images of SpyC-ADF3-SpyC protein under ammonium acetate buffer in pH 7.0. Scale bar is 20 µm. NTD represents for N-terminal domain from *Euprosthenops australis* MaSp1, CTD represents for C-terminal domain from *Araneus ventricosus* MiSp, SpyC represents for SpyCatcher002, CBM represents for cellulose binding domain, SilkC represents for SilkCatcher, and ADF3 represents for a wild type spidroin repetitive sequence from *Araneus diadematus* Fibroin-3.

Supporting Information). Isolated clusters of tiny compact granules, instead of the continuous network of SpyC-ADF3-SpyC, formed when adding 1.25 M ammonium acetate to 5 mg ml^{-1} CBM-ADF3-CBM protein. Similarly, 0.5 M potassium phosphate induced clusters of dense tiny droplets of CBM-ADF3-CBM, rather than droplets of LLPS that fuse together. Differences in the dimerization of terminal domains in triblock proteins have been reported to affect their phase-separation behavior.[56] Weak dimerization between CBMs have been reported, while no dimerization was observed for SpyC.[57] NTD-ADF3-CTD formed amorphous aggregates under all tested conditions (Figure S7, Supporting Information). This contrasts with previous reports on silk

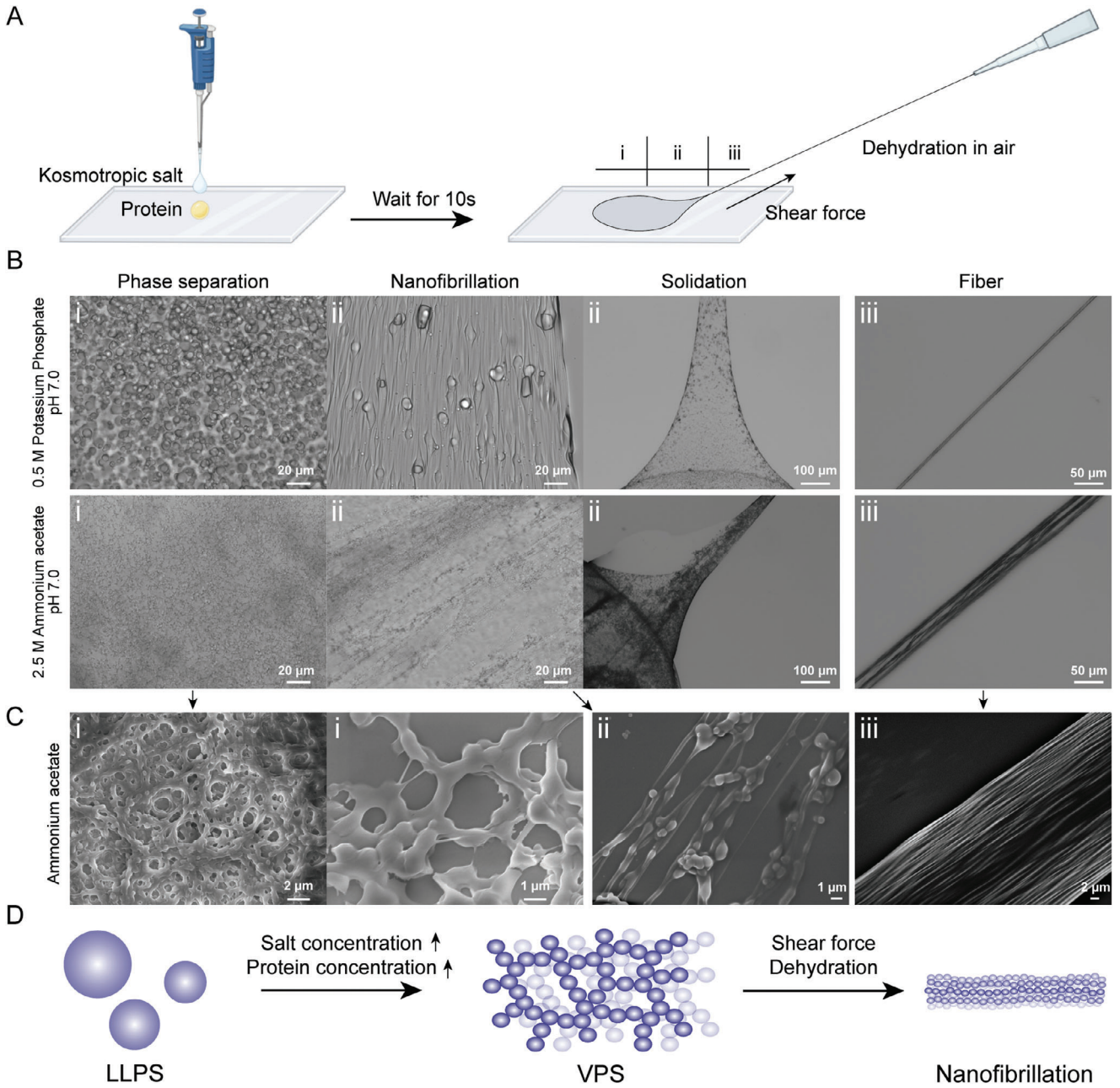

Figure 2. Phase separation and fiber formation of SpyC-ADF3-SpyC protein. A) Schematic presentation of the phase separation and fiber formation process. B) Different phase separation states and manually drawn fibers formed by SpyC-ADF3-SpyC in 0.5 M potassium phosphate and in 2.5 M ammonium acetate. Scale bars are 20, 100, and 50 µm. C). SEM images of the granule-based assembly process of SpyC-ADF3-SpyC induced by 2.5 M ammonium acetate. D) Schematic of protein phase separation and fiber formation of SpyC-ADF3-SpyC induced by salting out, shear force, and dehydration.

repeat sequences fused with NTD and CTD.[51,52] We attribute this difference to the differences in the silk repeat sequences used, affecting, for example, the solubility of the fusion proteins.

2.3. Fiber Formation Occurs via Phase-Separated Assemblies

Next we wanted to study the differences in the phase separation of SpyC-ADF3-SpyC in different salts and their effects on fiber assembly. To mimic the spider spinning process, [7,8] we applied shear force and dehydration by manually pulling fibers from the solution (Figures 2 and 3; Video S1, Supporting Information). Indeed, it was possible to draw fibers from the phase-separated SpyC-ADF3-SpyC or SilkC-ADF3-SilkC protein in very low (10 mg mL^{-1}) protein concentration either in 2.5 M ammonium acetate or 0.5 M potassium phosphate (**Figure 2A**; Figure S8, Supporting Information). However, when either the salt or protein concentration decreased, phase-separation did not take

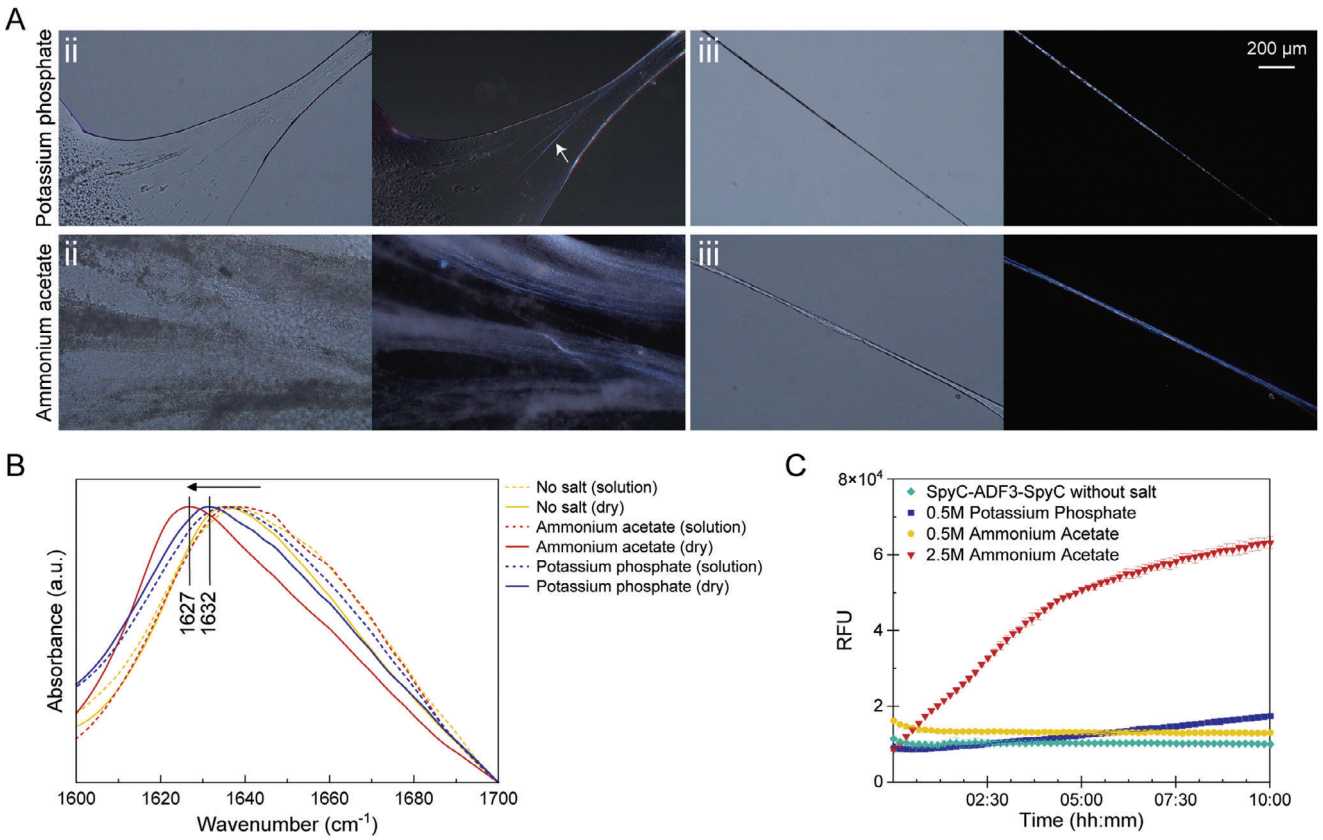

Figure 3. Probing molecular level changes of the silk protein assembly process. A) Polarized optical microscopy images of the two types of phase separations and fibers in different buffers. White arrows pointed to the tiny nanofiber induced by shear force. B) FTIR spectra of silk protein in: (i) 10 mg ml^{-1} protein in Milli-Q water, (ii) dry sample of 10 mg ml^{-1} protein (Milli-Q), (iii) 10 mg ml^{-1} protein in 2.5 M ammonium acetate, (iv) dry sample of 10 mg ml^{-1} protein (2.5 M ammonium acetate), (v) 10 mg ml^{-1} protein in 0.5 M potassium phosphate, (vi) dry sample of 10 mg ml^{-1} protein (0.5 M potassium phosphate). The black arrow points to the peak shift trend. The peaks of sample iv and vi in 1627 and 1632 cm^{-1}, respectively, are shown. C) ThT assay shows the timescale of the salt-induced cross β-sheet formation.

place, and consequently, fibers could not be drawn. CBM-ADF3-CBM, which exhibited tight phase separation with isolated cluster of protein granules, was unable to form fibers under the conditions tested. Our hypothesis is that the separated clusters formed during phase separation lacked connections between each other, preventing the formation of the network necessary for fiber formation.[58]

Nanofibrillation along the pulling direction occurred in the intermediate region between the fibers and droplets. In potassium phosphate, the protein droplets formed by LLPS were deformed and broken down by shear forces, then elongated into tiny nanofibrils (Figure 2B). In contrast, we observed that the droplet formed via VPS induced by ammonium acetate fused and deformed, and the nanofibers were highly ordered and appeared as bundles of nanofibers, accompanied by the fusion of fibers (Figure 2C,D). Scanning electron microscopy (SEM) of VPS observed in ammonium acetate revealed a network of droplets (Figure 2C). Inspection of the nanofibrillated region revealed how the network of droplets deformed into nanofibrils upon applying shear forces and dehydration. The hierarchical structure remained visible in the SEM images of the pulled fiber, which showed bundles of microfibers formed from the deformation and fusion of granules (Figure 2C). On the contrary, the fibers from LLPS triggered by potassium phosphate had a uniform surface without hierarchical structure (Figure S9, Supporting Information).

To further elucidate the molecular level changes, we studied the increasing degree of order and changes in secondary structure in the different steps of the fiber assembly. No birefringence was observed for the phase-separated solution of protein, indicating that phase separation alone was not sufficient to align the molecules (Figure S10, Supporting Information). Instead, the strong birefringence of the granules deformed under the shear forces was observed, indicating increased alignment of the molecules and the appearance of a crystalline phase (**Figure 3**A). While only tiny and crystallized microfibers marked with white arrow in Figure 3A are detectable from LLPS sample, bundles of crystallized microfibers were observed in ammonium acetate induced VPS sample (Figure 3A). Polarized optical microscopy of manually drawn fibers from both conditions showed birefringence, indicating good alignment of the protein chains in the fibers, essential for their mechanical properties. The secondary structure transition toward β-sheet structures that occurs during spider silk spinning was observed by FTIR spectroscopy and using a ThT assay (Figure 3B,C). There was no significant peak shift in the FTIR spectrum between protein in Milli-Q water or

kosmotropic salts, suggesting no transition in the secondary structures took place in the initial phase separation state (Figure 3B). However, the ThT assay indicated that the protein adopted cross β-sheet structure [59] over time in the presence of salt (Figure 3C). In accordance, the FTIR spectra of dried phase-separated samples had a peak shift. The ammonium acetate buffer-induced phase separation sample had a strong peak in 1627 cm^{-1}, while the phase-separated sample induced by potassium phosphate showed a strong peak in 1632 cm^{-1}, which attributed to β-sheet conformation [60–63] (Figure 3B). We conclude that shear forces and dehydration were required for both the alignment of the molecules and the secondary structure transition.

According to current model, spider major ampullate silk assembles in a process involving three steps.[64] First, LLPS with low ordered structure takes place in the sac of spider silk gland. This is followed by increasing alignment into hierarchical microstructures in liquid crystalline granules occurring during the spinning process in the tapering duct. Finally, granule-based microfibrils bundle and align along with the final fiber axis. Despite the differences in the molecular structure and spinning process, the ultrastructural assembly process that we observed with SpyC-ADF3-SpyC (Figures 2 and 3) and SilkC-ADF3-SilkC (Figure S4, Supporting Information), when triggered by ammonium acetate, shear force, and dehydration, resembles that occurring in spiders. The results indicate the potential for more universal principles of fiber spinning.[7]

2.4. Aqueous Spinning of Tough and Extensible Artificial Spider Silk Fibers

The mechanical properties of manually drawn fibers were moderate and the variation among the fibers measured was large (Figure S11, Supporting Information). The mechanical properties of the tested samples from different positions of one single drawn fiber varied significantly. Regions from the middle of the fibers pulled from VPS showed outstanding extensibility, ≈175%, while those from the end of the same fiber showed bad extensibility and higher strength. Fibers from LLPS droplets were all poorly extensible. Inefficient and uncontrollable shearing, dehydration, and extension processes inherent to the manual fiber pulling account for the uneven fibers and poor performance. We assumed that the fiber would be improved if the shearing could be processed with a constant speed and force, while the fiber shape can be controlled by a tube shape like spider spinning taper.

To tackle the problem of manually drawn fibers, wet spinning with a precise controllable process was applied to produce uniform and continuous fibers. The spinning conditions used here were selected to be mild and the spinning was conducted at ambient temperatures without using noxious chemicals as solvents or in the coagulation bath. The key requirements for wet spinning are a highly concentrated protein dope solution and a fast coagulation step. The globular terminal domains, SpyC, SilkC, and CBM, improve the solubility of recombinant proteins to 100–150 mg mL^{-1} in an aqueous solution which is sufficient for a dope solution. Most of the recombinant spider silk-like proteins without soluble NTD and/or CTD are insoluble in aqueous solution and have poor solubility even in organic solvent, except the mini-spidroin NT2RepCT and its variants which have short repetitive region and availability of two soluble terminal domains.

The transition of the protein SpyC-ADF3-SpyC from liquid state to VPS to nanofibrillation is very fast within seconds when induced by 2.5 M ammonium acetate in pH 7.0 and shear force. We therefore hypothesized that the neutral 2.5 M ammonium acetate would be an efficient coagulation bath to solidify the highly concentrated proteins into fiber. Indeed, the 2.5 M ammonium acetate coagulation bath produced continuous and collectable, but weak fibers. Increasing the concentrations of ammonium acetate (3 M or 4 M) resulted in hundreds of meters of continuous and stronger fibers. Fibers spun in 3 M ammonium acetate were more elastic, while those spun in 4 M ammonium acetate had higher strength yet lower toughness modulus (Figure S12, Supporting Information). Considering the environmental and economic perspective, we selected 3 M ammonium acetate, pH 7.0, for further experiments (**Figure** 4A). Collecting fibers at a higher collection rate, 100 cm s^{-1}, resulted in fibers with smaller diameter, increased strength, and Young's modulus, yet reduced strain and toughness modulus, compared to the fibers collected in 50 cm s^{-1} (Figure S13, Supporting Information). The results are in line with the existing literature stating that high collection rates cause fibers to stretch, causing low extensibility.[65–67]

All recombinant proteins constructed were used for wet spinning, except NTD-ADF3-CTD due to its poor yield and solubility. SpyC-ADF3-SpyC and SilkC-ADF3-SilkC proteins produced uniform and continuous fibers that could be collected by collection wheels for hundreds of meters in length (Figure 4B,C; Video S2, Supporting Information), while the CBM-ADF3-CBM fibers were too weak to be collected. The results are consistent with the results from manually drawn fibers after salting out induced phase separation, pointing out a potential way to screen for suitable spinning conditions in small scale.

The as-spun SpyC-ADF3-SpyC fibers showed an extraordinary extensibility, ≈255%, which is highest among as-spun recombinant major ampullate spider silk fibers (Figure 4D,E; Table S1, Supporting Information). The mechanical properties of spider silk mainly rely on the repeat units of the repetitive region, especially the length and combination of poly-A motifs.[31,38,68] Compared to other major ampullate silk proteins, ADF3 contains both $(GPGXX)_n$ and $(GGX)_n$ motifs while but only short poly-A motif where the number of alanines is 6. The motifs $(GPGXX)_n$ and $(GGX)_n$ presumably fold into β-spirals and 3_1 helices structures, respectively, which mainly contribute to the elasticity of the fiber.[13,44,69] The sequence of the repetitive region is likely the reason for the high extensibility of SpyC-ADF3-SpyC fibers. The toughness modulus of SpyC-ADF3-SpyC fibers is comparable to native spider dragline silk (120 and 129 MJ m^{-3}, respectively, compared to native MA silk of *A. diadematus* [31]) and outperforms most of the recombinant as-spun silk fibers, except the variant of NT2RepCT, $(A_3I)_3$-A_{14} [38] (Figure 4D,F; Table S1, Supporting Information). Typically, spidroins have a very high molecular weight, >250 kDa, and exceptionally long repeat regions,[30] and increasing the molecular weight of the silk-like proteins has been shown to improve the strengths of the resulting fibers, especially of the post-spun stretched fibers.[4,27–29,35,70] Direct comparison of the molecular weights of different spider silk fusion proteins and the mechanical properties of the fibers is, however,

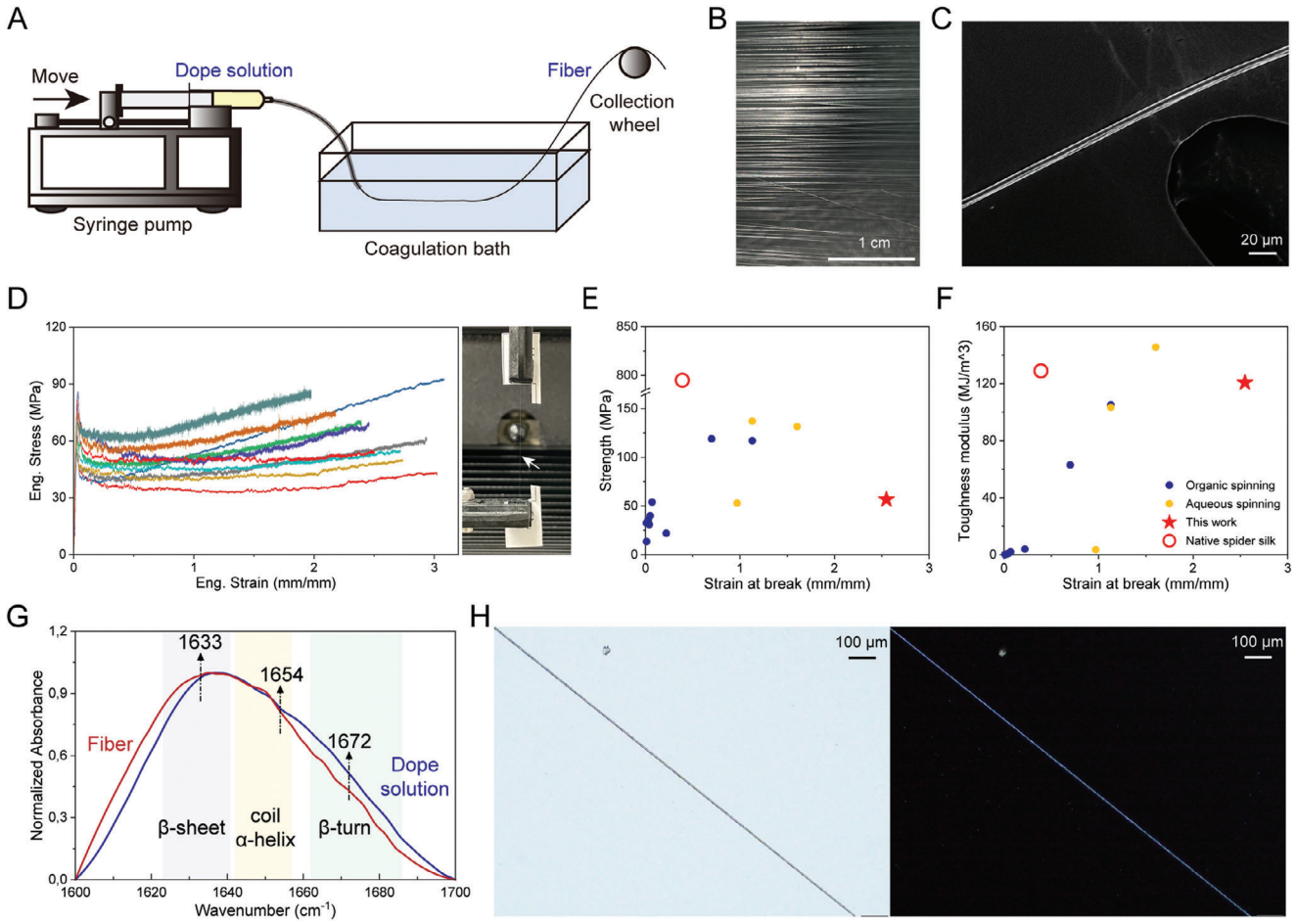

Figure 4. Artificial spider silk fibers with high toughness and extensibility produced by an aqueous system. A) Schematic of the wet spinning system used. B) Photograph of SpyC-ADF3-SpyC fibers. Scale bar: 1 cm. C) SEM image of an as-spun SpyC-ADF3-SpyC fiber. Scale bar: 20 μm. D) Representative tensile test curves of SpyC-ADF3-SpyC fibers, n = 10. E) and F) Strength-strain plot and toughness-strain plot for various as-spun artificial spider silk fibers and native dragline spider silk fibers. Blue dots represent as-spun fibers produced with organic solvent, such as ethanol, methanol, and isopropanol; yellow dots represent as-spun fibers produced with aqueous spinning; red circles represent natural dragline silk fibers; the red star is from SpyC-ADF3-SpyC fiber of this work. Data and references are listed in Table S1 (Supporting Information). G) FTIR spectrum of dope solution and as-spun fiber. The expected region of β-sheet conformation (1623–1641 cm^{-1}, average absorption band in 1633 cm^{-1}) is highlighted with gray shading, while the yellow shading indicates the region of random coil and α-helix conformations (1642–1657 cm^{-1}, average absorption band in 1654 cm^{-1}), and green shading that for the β-turn conformation (1662–1686 cm^{-1}, average absorption band in 1672 cm^{-1}).[62] H) Polarized microscopy image of fiber. Scale bar: 100 μm.

difficult due to the differences in the silk repeat sequences, terminal domains, spinning and testing conditions, as well as possible polymerization during spinning (Table S1, Supporting Information, and refs. [4,71–74]).

ATR-FTIR, polarized optical microscope, and XRD was used to investigate the degree of molecular orientation and secondary structure content of the SpyC-ADF3-SpyC fibers. The degree of alignment and the ratio of the crystalline and amorphous phases are key determinants of spider silk fiber properties.[63,75] Comparing the FTIR spectrum of dope solution and fiber of SpyC-ADF3-SpyC, a shift of a peak from 1637 to 1635 cm^{-1} was observed, indicative of increased β-sheet content and decreased contributions of α-helix/random coil conformations (Figure 4G; Figure S14; Table S2, Supporting Information). β-sheet content has a strong correlation with the mechanical properties of the fiber and typically strongly depends on the repeat region sequence [4,38,68] as well as the spinning process.[27,74] Sequences with less alanine-rich regions typically have lower β-sheet content leading to lower strength but higher extensibility and toughness modulus.[31,76] However, alanine-rich regions only increase the strength if post-stretching is applied, likely due to the limited secondary structure transition and poor alignment occurring during the spinning.[4] The polarized microscope images indicated a high degree of order in fibers (Figure 4H). In addition, XRD pattern of fibers were similar as previously reported in the literature,[74,77,78] showing a semi-crystalline structure (Figure S15, Supporting Information). The calculated crystallinity was 44.89%. Spider silk fibers are reported to have a hierarchical architecture in which the β-sheet nanocrystals are embedded in an amorphous matrix.[63,74,79] When the native fibers are subjected to stretching, reversible deformation and extension of the amorphous matrix occurs first, followed by irreversible deformation of the β-sheet crystals until the fiber breaks.[80,81] The alignment of the molecular and semi-crystalline

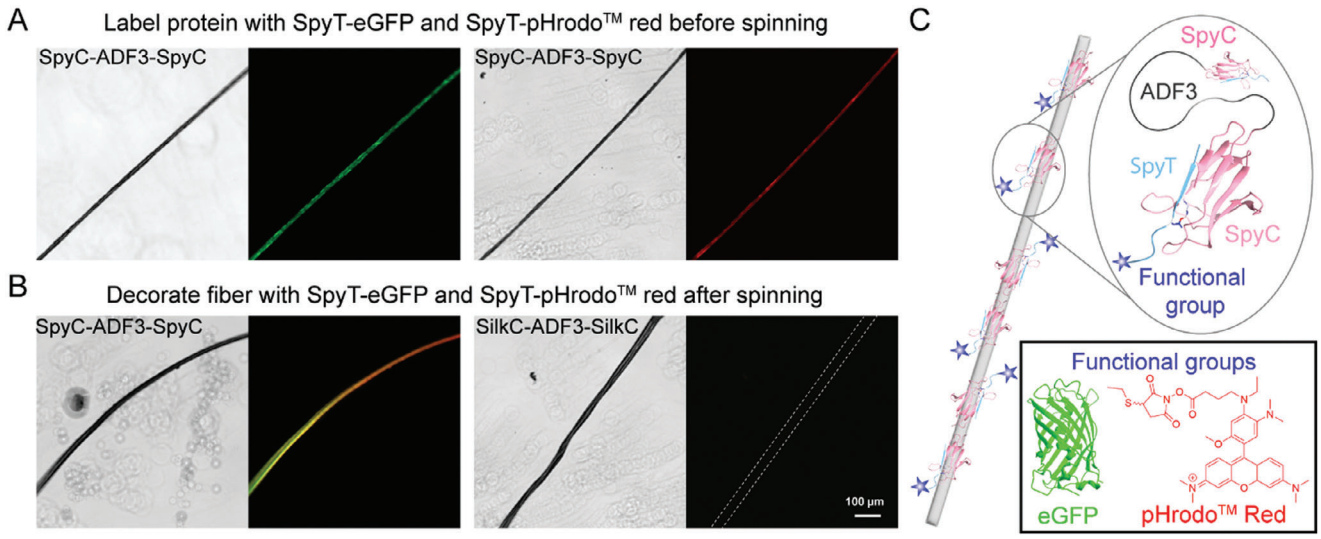

Figure 5. Specific and efficient functionalization through a biomolecular click reaction. A) Functionalization by conjugating SpyC-ADF3-SpyC protein with labeled SpyTag before spinning. B) Decorate fibers by soaking as-spun fiber in labeled SpyTag solutions. C) Schematic presentation of the production of functionalized fibers via a biomolecular click reaction. Scale bar: 100 μm.

structures is crucial for the mechanical properties of the fiber.

2.5. Functionalization by Biomolecular Click Reaction

Outstanding mechanical properties and biocompatibility make spider silk fiber a promising alternative for developing functional materials. Catcher/Tag pairs enable protein conjugation via an isopeptide-bond mediated biomolecular click-reaction.[82] The irreversible and efficient ligation takes place autocatalytically in a wide range of mild conditions, even with micromolar precursor concentration.[40,83] Several Catcher/Tag pairs have been reported from different split domains.[41] Despite the high structural similarity, the click reaction between Catcher and Tag is remarkably selective. Catcher/Tag pairs from different split domains generally have no cross-reactivity, for example, SdyCatcher/Tag pairs and SpyCatcher/Tag pairs,[84] SilkCatcher/Tag pairs and SpyCatcher/Tag pairs.[47] Here, we employed SpyCatcher2, which is an improved version of SpyCatcher with SpyTag, and SilkCatcher as globular terminal domains to produce recombinant spider silk fibers by the aqueous spinning system. We assumed that the Catchers remained active under the mild spinning process.

Thus, we employed two types of functionalization groups, an enhanced green fluorescent protein (eGFP) with a molecular weight of 26 kDa, and a small fluorescent probe, pHrodo red, to investigate the possibility to functionalize the fibers through the Catcher/Tag click reaction (Figure S16, Supporting Information). SpyTag was fused with eGFP by genetic engineering to generate SpyTag-eGFP, while pHrodo red was conjugated with a synthetic SpyTag peptide via a thiol reaction.

The fibers can be decorated by two simple methods both pre- and post-spinning. For pre-spinning labelling, we labeled the SpyC-ADF3-SpyC dope solution to spin functionalized fibers. The eGFP labeled fibers were not possible to be spun and collected in a continuous process, while the pHrodo red labeled could be collected, likely because the size of functionalized group affects the spinnability of SpyC-ADF3-SpyC (**Figure 5A**). The post-spinning decoration process was much simpler than the pre-spinning strategy and would likely also be easier to scale up. The as-spun fibers were submersed in labeled SpyTag solution overnight and washed by Milli-Q and 1% Triton X-100 with 2 cycles to remove unspecific binding. The decorated SpyC-ADF3-SpyC fibers showed a strong fluorescence (Figure 5B; Figure S17, Supporting Information). As a control, we employed the same post-spinning labeling process to SilkC-ADF3-SilkC fibers which did not show detectable fluorescent at the same fluorescent beam intensity, since the SilkCatcher has no cross-reaction activity with SpyTag (Figure 5B). These results indicate that functionalization through the biomolecular click reaction is very specific and offers potential to produce multifunctional spider silk fibers in a mild and efficient way (Figure 5C). Optimizing the parameters of the spinning and post-spinning processing, including the temperature of the coagulation bath,[85] humidity-induced supercontraction,[73,86] and introduction of crosslinked networks,[4] that are reported to have considerable effects on the mechanical properties of the fibers provide future possibilities for the optimization of the fiber properties. The process of functionalization provides additional possibilities for post-spinning processing.

We have demonstrated here the design of recombinant spider silk fusion protein that can be processed into fibers with excellent toughness and inherent potential for functionalization in a fully aqueous system (**Figure 6**). Previously reported aqueous spinning systems have relied on fusing the native terminal domains from spider silk proteins, NT and CT, with repetitive spider silk sequences (Table S1, Supporting Information). Instead of NT and CT, we fused repetitive silk sequence with two SpyCatcher domains. The resulting fusion protein could be produced recombinantly in *E. coli* and processed into fibers via a fully aqueous pathway, paving the way to establishing aqueous spinning

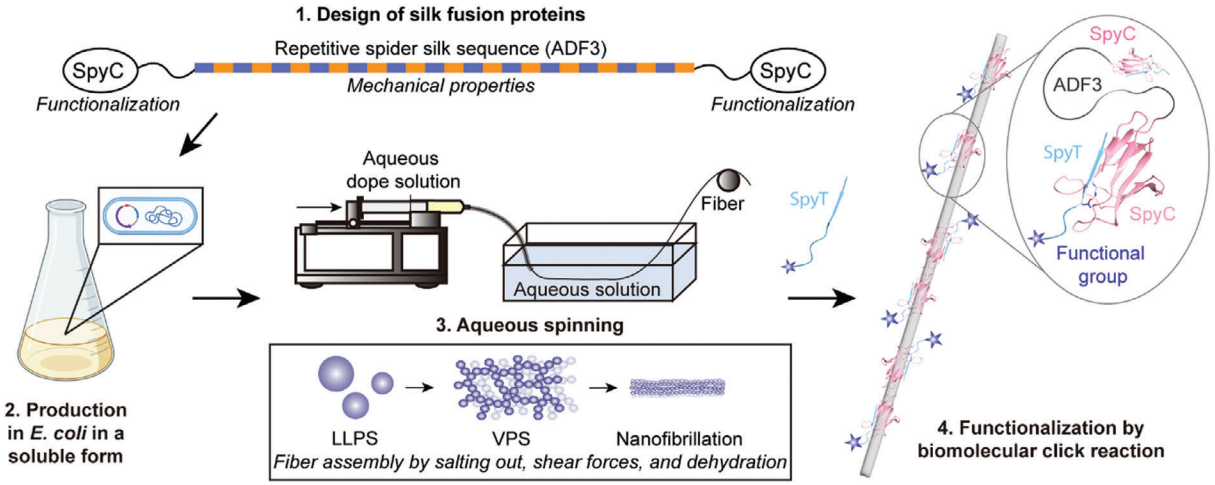

Figure 6. Schematic presentation of the design and production of recombinant spider silk with excellent toughness and inherent potential for functionalization. Fusing repetitive sequence of a wild-type spidroin, ADF3, with SpyCatcher domains, allows the spider-silk fusion protein to be expressed in a soluble manner and stored in aqueous dope solutions with high concentration. Salting-out induced assembly of the spider-silk fusion protein not only demonstrated ultrastructural similarity of assembly behavior to that of natural spider silk, but also enables aqueous wet spinning to produce fibers. The intrinsic properties of the SpyCatcher domains allow functionalization of the fiber by a biomolecular click reaction between SpyCatcher and SpyTag under mild conditions.

processes for spider silk fusion proteins with non-native terminal domains. The salting-out induced assembly resembles ultrastructurally that of native spider silks and results in fibers that have toughness comparable to that of native silk. Moreover, the fibers could be functionalized either pre- or post-spinning. We demonstrated the functionalization using a fluorescent protein, eGFP, as well as with a synthetic dye, pHrodo red. The resulting fluorescent fibers hold the potential for applications in particular in bioimaging.[87–89] In addition, due to the generality of the biomolecular click reaction mediated by the Catcher/Tag pair, the two functional groups used here, eGFP and pHrodo red, could be replaced by a large variety of different recombinant proteins or synthetic probes.

3. Conclusion

We demonstrated a simple "salting out-shear stress-dehydration" process to mimic the natural spinning process applied to spin fibers from a spider-silk fusion protein. We showed that the phase separation step was essential for the fiber spinning and the type of the phase separation affected the assembly process and fiber properties. Dehydration and mechanical stress-induced deformation were crucial for the transition into β-sheets and the alignment of the protein molecules into the liquid crystalline form required for continuous spinning. We applied the process to develop a sustainable aqueous wet spinning method and successfully produced the most extensible recombinant spider silk fibers with remarkable toughness. Finally, we functionalized these fibers via a highly selective and efficient biomolecular click reaction under mild conditions, which provides the possibility for the development of multifunctional 1D materials.

4. Experimental Section

Recombinant Spider Silk Protein Design, Expression, and Purification: The protein expression was performed in *E. coli* T7 express strain (NEB) using EnPresso media according to the protocol of the manufacturer (EnPresso B 500, EnPresso GmbH) at 30 °C (16 °C for NTD-ADF3-CTD). After 24 h of induction with Isopropyl β-d-1-thiogalactopyranoside (IPTG, final concentration 200 µM), the cells were harvested (12000 g for 20 min) and resuspended in 50 mM Tris-HCl buffer pH 7.4 containing 3 mM $MgCl_2$, 100 mM NaCl, 1 mg ml^{-1} Lysozyme (EC 3.2.1.17, Merck), 10 µg ml^{-1} DNAse I (EC 3.1.21.1, Merck) and 1 protease inhibitor tablet/50 ml buffer (Thermo Fisher Scientific). The resuspended cells were incubated for 1 h at 37 °C and 150 rpm followed by sonication (Qsonica 500, Qsonica LLC), for 4 × 2 min with 30% amplitude. The lysate was centrifuged at 15000 g for 30 min at RT and the supernatant was collected. The collected supernatant was purified by a Ni-immobilized metal affinity column (IMAC) (Äkta Pure, GE Healthcare, USA). After loading the supernatant on a 5 mL prepacked HisTrap FF (Cytiva, USA), the column was washed with 20–25 column volumes (CV) of washing buffer (10 mM imidazole, 20 mM Tris-HCl, and 300 mM NaCl, pH 7.4). The protein was eluted with elution buffer (250 mM imidazole, 20 mM Tris-HCl, and 300 mM NaCl, pH 7.4). The buffer was exchanged with deionized water after purification using Econo-Pac 10DG gel filtration columns (Bio-Rad Inc.). The protein solution was frozen in liquid nitrogen and stored at −80 °C until further use.

Protein purity and identity was confirmed with 10% or 8–16% sodium dodecyl polyacrylamide gel electrophoresis and precision plus dual color protein standard (Bio-Rad). The gel was stained with Coomassie brilliant blue R-250 for 1 h and destained with a solution containing 48% acetic acid and 40% ethanol for several hours before imaging.

Turbidity Measurement: Turbidity was measured by Synergy H1 multimode microplate reader. Samples containing protein and salts with desired final concentrations were placed in 96-well plates with a final volume of 200 µl and allowed to equilibrate for 10 min. Measurements were taken over a 10-h period and the absorbance values were recorded with 5 min intervals at 600 nm. The sample was shaken for 2 s before each readout. The temperature was kept at room temperature. Backgrounds were subtracted from the measurement readouts.

Optical Microscopy: Phase separation was imaged by Axio Vert.A1 inverted optical microscope equipped with an AxioCam 503 color camera (Carl Zeiss, Germany). Samples for the phase diagram were prepared by mixing the protein (in Milli-Q water pH 7.0) with an appropriate buffer with the desired final concentration on a glass slide in 1:1 ratio.

Manually Drawn Fiber: 2 µL of 20 mg ml^{-1} recombinant spider-silk fusion protein solution was dropped onto a glass slide and covered by

2 µL salts solutions. The protein samples turned turbid immediately, and after 5–10 s, the spider silk-like fibers were carefully pulled by a tip from the solution and extended into air.

Scanning Electron Microscopy (SEM): Scanning electron microscopy was performed with Zeiss Sigma FE-SEM in variable pressure for all the samples. For phase separation samples, samples were made on glass slides and dried in air overnight. Then the glass slides were fixed on an aluminum stub with conductive carbon tape. For fibers, samples were placed on an aluminum stub with conductive carbon tape. All the samples were sputtered with a thin platinum/palladium layer prior to imaging.

Polarized Optical Microscopy: Polarized optical microscopy was performed with an Olympus BX53-P microscope (Olympus, Japan) equipped with U-PO3 polarizer. For phase separation samples, samples were prepared by dropping protein on the glass slide, covering it with salt solutions, and then manually drawing fiber. Images were taken from the start point of fibers in droplets and the middle part of fibers. For fiber samples, fibers were fixed on a paper frame and put on a glass slide.

Thioflavin T (ThT) Assay: Aggregation kinetics were monitored in bulk solution by measuring ThT fluorescence at an excitation wavelength of 440 nm and an emission wavelength of 485 nm by SynergyTM H1 multimode microplate reader. ThT was dissolved in Milli-Q water and centrifuged at 12 000 g for 2 min to make a 1 mM stock solution. Proteins and ThT solutions were mixed and equilibrated for 10 min before adding appropriate salt solutions. The final concentration of ThT is 20 µM. Samples were placed in black-walled and clear-bottom 96-well plates with a final volume of 200 µl and allowed to equilibrate for 10 min before measurement. Measurements were taken over a 10-h period and the absorbance values were recorded with 5 min intervals at 600 nm. The sample was shaken for 2 s before each readout. The temperature was kept at room temperature. Backgrounds were subtracted from the measurement readouts.

Attenuated Total Reflectance Fourier Transform Infrared Spectroscopy (ATR-FTIR): A Unicam Mattson 3000 FTIR spectrometer equipped with PIKE Technologies GladiATR (with diamond crystal plate) was used for recording FTIR. All spectra were scanned within the range of 800–4000 cm^{-1}, with a total of 64 or 128 scans and a resolution of 1 or 2 cm^{-1}. For protein solution and phase separation samples, samples were directly dropped on the diamond crystal plate without tip fixation. For fibers, two bundles of perpendicular fibers were covered on the diamond crystal plate, a flat tip was used to fix fibers with a small pressure to eliminate the force effect on fibers.[90] Before every sample spectrum measurement, a background spectrum was recorded.

To resolve the secondary structure of the protein solution and fibers, three spectra of each sample were averaged, and the baseline was subtracted from the amide I band (1700 to 1600 cm^{-1}). Seven selected Gaussian bands (intermolecular β-sheet (1613, 1622, and 1633 cm^{-1}), α-helix/ random coil (1651 cm^{-1}), other secondary structure (1669 and 1680 cm^{-1}), and antiparallel amyloid β-sheet (1695 cm^{-1})) were selected for fitting with freedom of $\pm$5 cm^{-1} all the peaks. The fitting analysis of the spectra was iterated until convergence, and a Chi-Square tolerance value of 10^{-8} was obtained. The relative secondary structure content was calculated by dividing the area of each fitted curve by the total area of all fitted curves.

Artificial Fiber Spinning: A syringe with Luer Lok tip (BD, USA) was filled with concentrated recombinant spider silk fusion proteins dissolved in 200 mM NacCl, 20 mM Tris-HCl, pH 7.4, typically ranging from 10 to 15% w/v. The syringe was connected to a 27G blunt needle (Braun, Germany), which was connected to a glass capillary (WPI, 1 mm/0.5 mm outer/inner diameter) via a Puri-Flex tubing. The capillaries were pulled (PN-31, Narishige) and cut by a microforge (MF-900 Narishige) to an inner diameter of between 45 and 60 µm. The proteins were extruded with a flow rate of 0.1 µL s^{-1} (neMESYS low-pressure syringe pump, Cetoni, Germany) into a coagulation bath (50 cm in length, containing 3 M ammonium acetate, pH 7.0). Recombinant fibers were collected in air on rectangle frames attached to a roller at constant speed 50 cm s^{-1}. Spinning was conducted at RT (≈22 ± 2 °C). Fibers were stored in a humidity chamber with 20% RH.

Tensile Test: Fibers were fixed into a self-adhesive label frame with a window (0.75 cm x 1 cm). The diameter of the fibers was measured by Axio Vert.A1 inverted optical microscope with 20x objective lens. To simplify the measurement, we assumed that the fibers have a circular cross-section. The diameter of fibers was calculated from 10 different positions in three pictures of a single fiber. Tensile tests were performed with Universal Tester Instron 5944 equipped with 5N load cell. All the fibers were tested at a strain-rate of 2 mm min^{-1} and a relative humidity was 43±2%. The number of fibers tested was not less than 10. The calculations of the strain, fracture strength, Young's modulus, and toughness modulus were following ref. [71]. In brief, the true engineering stress and strain were calculated. For Young's modulus, the slope of the initial linear region of the stress-strain curves was calculated. The area under the stress-strain curve for toughness modulus was calculated.

X-Ray Diffraction: Fiber crystallinity was determined by X-ray diffraction (XRD) using a PANalytical X'Pert Pro MPD Alpha 1 (Malvern, UK). The radiation wavelength is 1.5418 Å for Cu Kα. The generator was operated at 45 kV and 40 mA in the angle range of 5–40 °. The Step size is 0.013 ° with 100 s per step. Self-deconvolution of the XRD profiles was performed with OriginLab using Gaussian curve fitting. The degree of crystallinity is calculated by dividing the crystallized area by the total area. A bundle of fibers without stretch was tested.

Labeling of SpyTag: To functionalize the protein and fibers, a labeled SpyTag peptide was used for covalent conjugation with SpyCatcher2. SpyTag peptide powder was dissolved in 20 mM Tris-HCl, pH 7.4, and 1 mM Tris(2-carboxyethyl) phosphine hydrochloride (TCEP, Sigma) was added to reduce the disulfide bond. pHrodo Red Maleimide (Thermo Fisher Scientific) was dissolved in dimethyl sulfoxide (Sigma). The thiol-maleimide reaction between the SpyTag peptide and pHrodo Red Maleimide was performed overnight at 4 °C.

For pre-spinning functionalization, the SpyC-ADF3-SpyC protein was reacted with the labeled SpyTag peptide or eGFP-SpyTag protein at room temperature for 2 h. For post-spinning functionalization, as-spun fibers were immersed in the labeled SpyTag peptide and/or eGFP-SpyTag protein solution overnight. To remove unlabeled SpyTag peptide and eGFP-SpyTag protein, the labeled fibers were washed with Milli-Q water and 1% Triton X-100 for two cycles.

Fluorescent Microscope: Imaging was done with an Axio Observer Z1 (Carl Zeiss, Germany) microscope with Andor iXon Ultra 888 cameras. The GFP signal was obtained using excitation light at 470 nm while collecting the emitted light of 515–535 nm. The pHrodo Red signal was obtained using excitation light at 590 nm while collecting the emitted light of 610–635 nm. The z-stacks were collected with a spinning disk (on confocal mode) with 200 nm steps and 50% laser power by using a Nikon Ti-E inverted microscope equipped with a Crest Optics X-light V3 spinning disk confocal head.

Statistical Analysis: Statistical analyses were performed in OriginLab. Mean values ± STD are provided for the data. Sample size (n) is provided for each analysis. No analysis of significant differences was applied.

Supporting Information

Supporting Information is available from the Wiley Online Library or from the author.

Acknowledgements

The authors thank Yin Yin for kindly providing the plasmid coding for eGFP-SpyTag. This work was supported by the Academy of Finland project no. (333238), by the Academy of Finland's Center of Excellence Program (2022-2029) project no. (346105), as well as by the Novo Nordisk Foundation grant no. (NNF23OC0081564). R.F. acknowledges support from the Jenny and Antti Wihuri's fund grant no. (00230063). B.S. was supported by the Swedish Research Council for Sustainable Development, FORMAS (grant number 2023-00871). G.G. was supported by the project "EPASS" under the HORIZON TMA MSCA Postdoctoral Fellowships – European Fellowships (project number 101103616). A.R. was supported by the European Research Council (ERC) under the European Union's

Horizon 2020 Research and Innovation Program (grant agreement No. 815357), Olle Engkvist Foundation (207-0375), the Center for Innovative Medicine (CIMED) at Karolinska Institutet and Stockholm City Council, the Swedish Research Council (2019-01257) and FORMAS (2019-00427)

Conflict of Interest

The authors declare no conflict of interest.

Data Availability Statement

The data that support the findings of this study are available from the corresponding author upon reasonable request.

Keywords

aqueous wet spinning, biomolecular click reaction, phase separation, recombinant spider silk, salt out

Received: June 14, 2024
Revised: July 8, 2024
Published online: July 26, 2024

[1] F. Vollrath, D. P. Knight, *Nature.* **2001**, *410*, 541.
[2] P. Mohammadi, A. Sesilja Aranko, C. P. Landowski, O. Ikkala, K. Jaudzems, W. Wagermaier, M. B. Linder, *Sci. Adv.* **2019**, *5*, eaaw2541.
[3] A. Rising, M. Widhe, J. Johansson, M. Hedhammar, *Cell. Mol. Life Sci.* **2011**, *68*, 169.
[4] B. Schmuck, G. Greco, T. B. Pessatti, S. Sonavane, V. Langwallner, T. Arndt, A. Rising, *Adv. Funct. Mater.* **2023**, 2305040.
[5] J. Cheng, C. F. Hu, C. Y. Gan, X. X. Xia, Z. G. Qian, *ACS Biomater. Sci. Eng.* **2022**, *8*, 3299.
[6] J. Li, B. Jiang, X. Chang, H. Yu, Y. Han, F. Zhang, *Nat. Commun.* **2023**, *14*, 2127.
[7] A. Rising, M. J. Harrington, *Chem. Rev.* **2023**, *123*, 2155.
[8] L. Eisoldt, A. Smith, T. Scheibel, *Mater. Today.* **2011**, *14*, 80.
[9] J. Chen, A. Tsuchida, A. D. Malay, K. Tsuchiya, H. Masunaga, Y. Tsuji, M. Kuzumoto, K. Urayama, H. Shintaku, K. Numata, *Nat. Commun.* **2024**, *15*, 1.
[10] A. Rising, J. Johansson, *Nat. Chem. Biol.* **2015**, *11*, 309.
[11] A. Koeppel, N. Stehling, C. Rodenburg, C. Holland, A. Koeppel, N. Stehling, C. Rodenburg, C. Holland, *Adv. Funct. Mater.* **2021**, *31*, 2103295.
[12] K. Arakawa, N. Kono, A. D. Malay, A. Tateishi, N. Ifuku, H. Masunaga, R. Sato, K. Tsuchiya, R. Ohtoshi, D. Pedrazzoli, A. Shinohara, Y. Ito, H. Nakamura, A. Tanikawa, Y. Suzuki, T. Ichikawa, S. Fujita, M. Fujiwara, M. Tomita, S. J. Blamires, J. A. Chuah, H. Craig, C. P. Foong, G. Greco, J. Guan, C. Holland, D. L. Kaplan, K. Sudesh, B. B. Mandal, Y. Norma-Rashid, et al., *Sci. Adv.* **2022**, *8*, 6043.
[13] J. M. Gosline, P. A. Guerette, C. S. Ortlepp, K. N. Savage, *J. Exp. Biol.* **1999**, *202*, 3295.
[14] A. Simmons, C. A. Michal, L. W. Jelinski, *Science.* **1996**, *271*, 84.
[15] M. Xu, R. V. Lewis, *Proc Natl Acad Sci USA* **1990**, *87*, 7120.
[16] S. Keten, Z. Xu, B. Ihle, M. J. Buehler, *Nat. Mater.* **2010**, *9*, 359.
[17] A. Sponner, E. Unger, F. Grosse, K. Weisshart, *Biomacromolecules.* **2004**, *5*, 840.
[18] S. Schwarze, F. U. Zwettler, C. M. Johnson, H. Neuweiler, *Nat. Commun.* **2013**, *4*, 2815.
[19] W. A. Gaines, M. G. Sehorn, W. R. Marcotte, *J. Biol. Chem.* **2010**, *285*, 40745.
[20] N. Kronqvist, M. Otikovs, V. Chmyrov, G. Chen, M. Andersson, K. Nordling, M. Landreh, M. Sarr, H. Jörnvall, S. Wennmalm, J. Widengren, Q. Meng, A. Rising, D. Otzen, S. D. Knight, K. Jaudzems, J. Johansson, *Nat. Commun.* **2014**, *5*, 3254.
[21] K. Jaudzems, G. Askarieh, M. Landreh, K. Nordling, M. Hedhammar, H. Jörnvall, A. Rising, S. D. Knight, J. Johansson, *J. Mol. Biol.* **2012**, *422*, 477.
[22] F. Hagn, C. Thamm, T. Scheibel, H. Kessler, *Angew. Chem. – Int. Ed.* **2011**, *50*, 310.
[23] F. Hagn, L. Eisoldt, J. G. Hardy, C. Vendrely, M. Coles, T. Scheibel, H. Kessler, *Nature.* **2010**, *465*, 239.
[24] G. Askarieh, M. Hedhammar, K. Nordling, A. Saenz, C. Casals, A. Rising, J. Johansson, S. D. Knight, *Nature.* **2010**, *465*, 236.
[25] M. Landreh, G. Askarieh, K. Nordling, M. Hedhammar, A. Rising, C. Casals, J. Astorga-Wells, G. Alvelius, S. D. Knight, J. Johansson, H. Jörnvall, T. Bergman, *J. Mol. Biol.* **2010**, *404*, 328.
[26] M. Andersson, G. Chen, M. Otikovs, M. Landreh, K. Nordling, N. Kronqvist, P. Westermark, H. Jörnvall, S. Knight, Y. Ridderstråle, L. Holm, Q. Meng, K. Jaudzems, M. Chesler, J. Johansson, A. Rising, *PLoS Biol.* **2014**, *12*, 1001921.
[27] A. Heidebrecht, L. Eisoldt, J. Diehl, A. Schmidt, M. Geffers, G. Lang, T. Scheibel, *Adv. Mater.* **2015**, *27*, 2189.
[28] X. X. Xia, Z. G. Qian, C. S. Ki, Y. H. Park, D. L. Kaplan, S. Y. Lee, *Proc. Natl. Acad. Sci. USA* **2010**, *107*, 14059.
[29] C. H. Bowen, B. Dai, C. J. Sargent, W. Bai, P. Ladiwala, H. Feng, W. Huang, D. L. Kaplan, J. M. Galazka, F. Zhang, *Biomacromolecules.* **2018**, *19*, 3853.
[30] C. Thamm, T. Scheibel, *Biomacromolecules.* **2017**, *18*, 1365.
[31] M. Saric, L. Eisoldt, V. Döring, T. Scheibel, *Adv. Mater.* **2021**, *33*, 2006499.
[32] X. Qi, H. Wang, K. Wang, Y. Wang, A. Leppert, I. Iashchishyn, X. Zhong, Y. Zhou, R. Liu, A. Rising, M. Landreh, J. Johansson, G. Chen, *Adv. Funct. Mater.* **2024**, *34*, 2315409.
[33] Z. Lin, Q. Deng, X.-Y. Liu, D. Yang, Z. Lin, D. Yang, Q. Deng, X. Liu, *Adv. Mater.* **2013**, *25*, 1216.
[34] C. F. Hu, Z. G. Qian, Q. Peng, Y. Zhang, X. X. Xia, *ACS Biomater. Sci. Eng.* **2021**, *7*, 3608.
[35] H. Zhu, A. Rising, J. Johansson, X. Zhang, Y. Lin, L. Zhang, T. Yi, J. Mi, Q. Meng, *Int. J. Biol. Macromol.* **2020**, *154*, 765.
[36] M. Andersson, Q. Jia, A. Abella, X. Y. Lee, M. Landreh, P. Purhonen, H. Hebert, M. Tenje, C. V. Robinson, Q. Meng, G. R. Plaza, J. Johansson, A. Rising, *Nat. Chem. Biol.* **2017**, *13*, 262.
[37] B. Schmuck, G. Greco, A. Barth, N. M. Pugno, J. Johansson, A. Rising, *Mater. Today.* **2021**, *50*, 16.
[38] T. Arndt, G. Greco, B. Schmuck, J. Bunz, O. Shilkova, J. Francis, N. M. Pugno, K. Jaudzems, A. Barth, J. Johansson, A. Rising, *Adv. Funct. Mater.* **2022**, *32*, 2200986.
[39] P. Mohammadi, A. S. Aranko, L. Lemetti, Z. Cenev, Q. Zhou, S. Virtanen, C. P. Landowski, M. Penttilä, W. J. Fischer, W. Wagermaier, M. B. Linder, *Commun. Biol.* **2018**, *1*, 86.
[40] A. H. Keeble, A. Banerjee, M. P. Ferla, S. C. Reddington, I. N. A. K. Anuar, M. Howarth, *Angew. Chem. – Int. Ed.* **2017**, *56*, 16521.
[41] R. Fan, A. S. Aranko, *ChemBioChem.* **2024**, *25*, 202300600.
[42] A. Rising, G. Hjälm, W. Engström, J. Johansson, *Biomacromolecules.* **2006**, *7*, 3120.
[43] G. Chen, X. Liu, Y. Zhang, S. Lin, Z. Yang, J. Johansson, A. Rising, Q. Meng, *PLoS One.* **2012**, *7*, 52293.
[44] T. Scheibel, *Microb. Cell Fact.* **2004**, *3*, 1.
[45] N. Kronqvist, M. Sarr, A. Lindqvist, K. Nordling, M. Otikovs, L. Venturi, B. Pioselli, P. Purhonen, M. Landreh, H. Biverstål, Z. Toleikis, L. Sjöberg, C. V. Robinson, N. Pelizzi, H. Jörnvall, H. Hebert, K. Jaudzems, T. Curstedt, A. Rising, J. Johansson, *Nat. Commun.* **2017**, *8*, 1.
[46] L. Lemetti, A. Scacchi, Y. Yin, M. Shen, M. B. Linder, M. Sammalkorpi, A. S. Aranko, *Biomacromolecules.* **2022**, *23*, 3142.

[47] R. Fan, J. Hakanpää, K. Elfving, H. Taberman, M. B. Linder, A. S. Aranko, *Angew. Chem. – Int. Ed.* **2023**, *62*, 202216371.
[48] P. Mohammadi, J. Christopher, G. Beaune, P. Engelhardt, A. Kamada, J. V. I. Timonen, T. P. J. Knowles, M. Penttila, M. B. Linder, *J. Colloid Interface Sci.* **2020**, *560*, 149.
[49] J. Tormo, R. Lamed, A. J. Chirino, E. Morag, E. A. Bayer, Y. Shoham, T. A. Steitz, *EMBO J.* **1996**, *15*, 5739.
[50] N. A. Oktaviani, A. Matsugami, F. Hayashi, K. Numata, *Chem. Commun.* **2019**, *55*, 9761.
[51] A. D. Malay, T. Suzuki, T. Katashima, N. Kono, K. Arakawa, K. Numata, *Sci. Adv.* **2020**, *6*, eabb6030.
[52] A. Leppert, G. Chen, D. Lama, C. Sahin, V. Railaite, O. Shilkova, T. Arndt, E. G. Marklund, D. P. Lane, A. Rising, M. Landreh, *Nano Lett.* **2023**, *23*, 5836.
[53] U. Slotta, S. Hess, K. Spieß, T. Stromer, L. Serpell, T. Scheibel, *Macromol. Biosci.* **2007**, *7*, 183.
[54] M. Humenik, A. M. Smith, S. Arndt, T. Scheibel, *J. Struct. Biol.* **2015**, *191*, 130.
[55] H. Tanaka, *Commun. Phys.* **2022**, *5*, 1.
[56] I. Tunn, G. Beaune, J. Tersteegen, T. Välisalmi, J. V. I. Timonen, F. Brochard-Wyart, M. B. Linder, *Commun. Phys.* **2024**, *7*, 1.
[57] D. Fedorov, N. Roas-Escalona, D. Tolmachev, A. L. Harmat, A. Scacchi, M. Sammalkorpi, A. S. Aranko, M. B. Linder, *Small.* **2024**, *20*, 2306817.
[58] S. Rammensee, U. Slotta, T. Scheibel, A. R. Bausch, *Proc. Natl. Acad. Sci. USA* **2008**, *105*, 6590.
[59] M. Biancalana, S. Koide, *Biochim. Biophys. Acta.* **2010**, *1804*, 1405.
[60] J. Zhong, Y. Liu, J. Ren, Y. Tang, Z. Qi, X. Zhou, X. Chen, Z. Shao, M. Chen, D. L. Kaplan, S. Ling, *ACS Biomater. Sci. Eng.* **2019**, *5*, 3161.
[61] S. Ling, Z. Qi, D. P. Knight, Z. Shao, X. Chen, *Biomacromolecules.* **2011**, *12*, 3344.
[62] A. Barth, *Biochim. Biophys. Acta (BBA) – Bioenerget.* **2007**, *1767*, 1073.
[63] Q. Wang, P. McArdle, S. L. Wang, R. L. Wilmington, Z. Xing, A. Greenwood, M. L. Cotten, M. M. Qazilbash, H. C. Schniepp, *Nat. Commun.* **2022**, *13*, 4329.
[64] T. Y. Lin, H. Masunaga, R. Sato, A. D. Malay, K. Toyooka, T. Hikima, K. Numata, *Biomacromolecules.* **2017**, *18*, 1350.
[65] R. J. Young, C. Holland, Z. Shao, F. Vollrath, *MRS Bull.* **2021**, *46*, 915.
[66] F. Vollrath, B. Madsen, Z. Shao, *Proc. Biol. Sci.* **2001**, *268*, 2339.
[67] B. Schmuck, G. Greco, F. G. Bäcklund, N. M. Pugno, J. Johansson, A. Rising, *Commun. Mater.* **2022**, *3*, 83.
[68] C. F. Hu, C. Y. Gan, Y. J. Zhu, X. X. Xia, Z. G. Qian, *ACS Biomater. Sci. Eng.* **2023**, *10*, 2925.
[69] J. D. Van Beek, S. Hesst, F. Vollrath, B. H. Meier, *Proc. Natl. Acad. Sci. USA* **2002**, *99*, 10266.
[70] Q. Jin, F. Pan, C. F. Hu, S. Y. Lee, X. X. Xia, Z. G. Qian, *Metab. Eng.* **2022**, *70*, 102.
[71] G. Greco, B. Schmuck, S. K. Jalali, N. M. Pugno, A. Rising, *Biophys. Rev.* **2023**, *4*, 31301.
[72] T. Vehoff, A. Glišović, H. Schollmeyer, A. Zippelius, T. Salditt, *Biophys. J.* **2007**, *93*, 4425.
[73] K. Yazawa, A. D. Malay, H. Masunaga, Y. Norma-Rashid, K. Numata, *Commun. Mater.* **2020**, *1*, 1.
[74] N. Du, Y. L. Xiang, J. Narayanan, L. Li, M. L. M. Lim, D. Li, *Biophys. J.* **2006**, *91*, 4528.
[75] J. Pérez-Rigueiro, M. Elices, G. R. Plaza, G. V. Guinea, *Molecules.* **2021**, *26*, 1794.
[76] K. Z. Htut, A. M. Alicea-Serrano, S. Singla, I. Agnarsson, J. E. Garb, M. Kuntner, M. Gregorič, R. A. Haney, M. Marhabaie, T. A. Blackledge, A. Dhinojwala, *J. R. Soc. Interface.* **2021**, *18*, 20210320.
[77] S. Sampath, J. L. Yarger, *RSC Adv.* **2014**, *5*, 1462.
[78] J. O. Warwicker, *J. Mol. Biol.* **1960**, *2*, 350.
[79] A. Nova, S. Keten, N. M. Pugno, A. Redaelli, M. J. Buehler, *Nano Lett.* **2010**, *10*, 2626.
[80] M. Wang, Z. Yang, C. Wang, M. Si, *J. Mol. Struct.* **2022**, *1270*, 133933.
[81] T. Giesa, M. Arslan, N. Pugno, M. Buehler, *Nat. Prec.* **2011**, *2011*, 1.
[82] G. Veggiani, B. Zakeri, M. Howarth, *Trends Biotechnol.* **2014**, *32*, 506.
[83] G. Veggiani, T. Nakamura, M. D. Brenner, R. V. Gayet, J. Yan, C. V. Robinson, M. Howarth, *Proc. Natl. Acad. Sci. USA* **2016**, *113*, 1202.
[84] L. L. Tan, S. S. Hoon, F. T. Wong, *PLoS One.* **2016**, *11*, 0165074.
[85] A. E. Albertson, F. Teulé, W. Weber, J. L. Yarger, R. V. Lewis, *J. Mech. Behav. Biomed. Mater.* **2014**, *29*, 225.
[86] Q. Dong, G. Fang, L. Hu, J. Yao, Z. Shao, X. Chen, Y. Huang, S. Ling, *J. Mater. Chem. B.* **2019**, *8*, 168.
[87] Z.-F. Wu, Z.-N. Sun, H.-M. Xiong, *Chin. J. Chem.* **2023**, *41*, 2035.
[88] S. Ling, Z. Qin, C. Li, W. Huang, D. L. Kaplan, M. J. Buehler, *Nat. Commun.* **2017**, *8*, 1.
[89] D. W. Kim, O. J. Lee, S. W. Kim, C. S. Ki, J. R. Chao, H. Yoo, S. il Yoon, J. E. Lee, Y. R. Park, H. Y. Kweon, K. G. Lee, D. L. Kaplan, C. H. Park, *Biomaterials.* **2015**, *70*, 48.
[90] M. J. Jafari, F. G. Bäcklund, T. Arndt, B. Schmuck, G. Greco, A. Rising, A. Barth, T. Ederth, *ACS Appl. Polym. Mater.* **2023**, *5*, 9433.